Lack of surface oxide layers and facile bulk oxide formation on Pd(110)

R. Westerström, C. J. Weststrate, J. Gustafson, A. Mikkelsen, J. Schnadt, J. N. Andersen, and E. Lundgren
Division of Synchrotron Radiation Research, Lund University, P.O. Box 118, 221 00 Lund, Sweden

N. Seriani, F. Mittendorfer, and G. Kresse
Fakultät Physik, Universität Wien, 1090 Wien, Austria

A. Stierle
Max-Planck Institut für Metallforschung, Heisenbergstr. 3, 70569 Stuttgart, Germany

(Received 2 June 2009; revised manuscript received 1 September 2009; published 30 September 2009)

The oxidation of the Pd(110) surface has been studied from ultrahigh vacuum up to atmospherical pressures by combining scanning tunneling microscopy, low-energy electron diffraction and high-resolution core-level spectroscopy with *in situ* surface x-ray diffraction, and density-functional theory calculations. Under *in situ* conditions, we observe a $c(2\times4)$ structure which transforms via the formation of antiphase domain boundaries to a "complex" structure with increasing partial oxygen pressure. Contrary to other closed packed and vicinal Pd surfaces investigated so far, no surface oxide is formed, which allows for the formation of the PdO bulk oxide closer to the thermodynamic limit at temperatures relevant for catalysis.

DOI: 10.1103/PhysRevB.80.125431 PACS number(s): 68.47.Gh, 61.05.cm, 68.37.Ef, 79.60.−i

I. INTRODUCTION

Pd is widely used for catalyzing oxidation and reduction reactions. An everyday application encountered by most people is the so-called Pd-only three-way catalyst (TWC) or Pd-Rh-based TWC,[1] which is used in the automotive industry to clean car exhausts. Despite a significant amount of research using ultrahigh vacuum (UHV) conditions the active phase of the Pd surface for CO oxidation, and further issues concerning the details of the reaction pathways, in particular under more realistic conditions,[2,3] are still under discussion.[4–13]

Previous investigations of late transition metal surfaces have shown that well-ordered ultrathin surface oxides[14–27] can form at elevated oxygen pressures, prior to the formation of bulk oxides.[17,25] It has also been shown in recent studies that the formation of oxide structures coincide with a large production of CO_2.[28–36] The determination of the different phases present on the surface under realistic conditions is therefore a central step toward an atomistic understanding of heterogeneous catalysis on single crystal surfaces.

Investigations of the interaction between the Pd(110) surface and oxygen gas started as early as 1969 with a low-energy electron diffraction (LEED) study by Ertl and Rau,[37] in which a series of ordered structures was described, $p(1\times3)$, $p(1\times2)$, $c(2\times4)$, $c(2\times6)$, and a "complex" structure. Since then, all of these structures have been the subject of numerous investigations.[37–52] The by far most studied structure is the $c(2\times4)$ reconstruction, for which experimental and theoretical investigations have resulted in an atomistic model.[48–51] For the $p(1\times3)$, $p(1\times2)$, and the $c(2\times6)$ structures different models have been proposed,[38,41,42,45] and recently a structural model was presented for the complex structure.[52] In most of these studies the different structures were formed by exposing the Pd(110) surface to oxygen gas at sample temperatures between −173 °C and room temperature (RT), and subsequently annealing the crystal to temperatures between RT and 530 °C. One exception of this preparation method can be found in Ref. 46 which report an *in situ* high-temperature STM study. In addition to these oxygen structures, *ex situ* studies have reported that bulk PdO forms on the surface at high partial oxygen pressures.[54,55]

Here we use traditional electron-based UHV techniques such as STM, LEED, and high-resolution core-level spectroscopy (HRCLS) together with DFT calculations to determine the atomic structure of the different phases present on the surface after oxygen exposure between 10^{-10} and 10^{-3} mbar. The obtained information was used with surface x-ray diffraction (SXRD) to identify the different phases under *in situ* conditions. We attempt to approach conditions at which a real catalyst operates by investigating the Pd(110) surface systematic at elevated partial oxygen pressures and sample temperatures (10^{-8}–10^{2} mbar at 270–390 °C). Our study shows that the surface forms a $p(1\times3)$ structure at 10^{-8} mbar and a sample temperature of 300 °C. The $p(1\times3)$ structure transforms via a $p(1\times2)$ to a $c(2\times4)$ structure within seconds at these conditions. The $c(2\times4)$ structure remains stable up to approximately 10^{-7} mbar of oxygen, above which it transforms via the formation of $c(2\times4)$ antiphase domain walls. As the density of these antiphase domain walls increase, the surface eventually forms the complex structure,[52] which at approximately 10^{-2} mbar transforms into the PdO bulk oxide.

II. EXPERIMENTAL AND COMPUTATIONAL SETUP

The HRCLS measurements were performed at beam line I311 (Ref. 56) at MAX-laboratory, Lund, Sweden, using a normal emission angle and photon energies of 390 eV for the Pd $3d_{5/2}$ and 625 eV for the O $1s$ levels. The data where fitted using a convolution of a Doniach and Šunjić[64] and a Gaussian line shape.

The SXRD measurements were carried out at the MPI-MF-beam line[57] at Angströmquelle Karlsruhe using photon energies of 10 and 8.92 keV, and at beam line ID03[58] at the

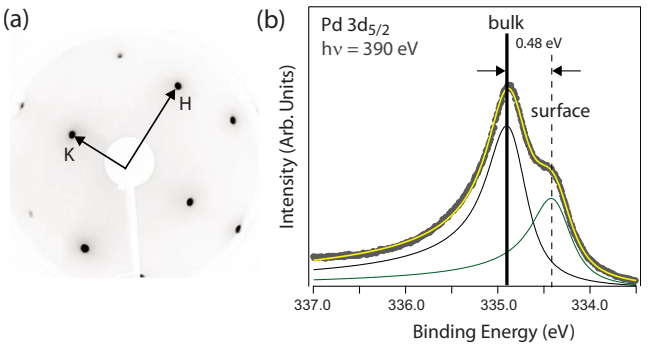

FIG. 1. (Color online) (a) LEED image of the clean Pd(110) surface. (b) HRCL spectrum from the Pd $3d_{5/2}$ level. The topmost atomic layer exhibits a SCLS of −0.48 eV.

European Synchrotron Radiation Facility (ESRF) using a photon energy of 17 keV. The experimental end stations for these beam lines are constructed specifically for studies under high pressures and at elevated sample temperatures. The crystal basis used to describe the (HKL) directions is a tetragonal basis, expressed in terms of the cubic Pd lattice, with $\mathbf{a}_1=1/2[-1,1,0]$ and $\mathbf{a}_2=[0,0,1]$ lying in the surface plane and $\mathbf{a}_3=1/2[1,1,0]$ out of plane. In this basis $\alpha=\beta=\gamma=90°$ and $a_0=3.89$ Å is the bulk Pd lattice constant. During the x-ray experiment, the sample temperature was measured by a Chromel Alumel thermocouple in direct contact with the crystal resulting in an absolute temperature uncertainty of ±5 °C. The oxygen pressure was monitored by a combination of a low pressure cold cathode gauge and two high pressure capacitive membrane gauges working from 10^{-3} to 1 mbar and from 1 mbar to 1 bar, respectively.

The STM images were recorded in Lund using a commercial Omicron STM1 positioned inside an ultra high vacuum system with a base pressure better than 1×10^{-10} mbar and operated at room temperature. All images shown were recorded in constant current mode using electrochemically etched tungsten tips.

The Pd(110) surface was cleaned by cycles of Argon sputtering, followed by annealing to approximately 800 °C. The crystal was also repeatedly heated and cooled in 10^{-7} mbar of oxygen, thereby removing any carbon contamination on the surface.

The calculations were performed within density-functional theory in the generalized gradient approximation with the PW91 exchange-correlation potential.[59] The electronic wave functions have been described by the projector-augmented-wave method of Blöchl[60] as implemented[61] in the Vienna *ab initio* simulation package.[62] The same simulation parameters as in Ref. 52 were employed. The core-level shifts were calculated including final-state contributions as described in Ref. 63.

III. THE CLEAN SURFACE

After extensive cleaning the HRCL spectrum showed no contaminations and the corresponding LEED image displayed a well-ordered (1×1) diffraction pattern, see Fig. 1(a). The Pd $3d_{5/2}$ spectrum shown in Fig. 1(b) can be decomposed into a bulk and a surface component with a surface core-level shift (SCLS) of approximately −0.48 eV. In the case of clean Pd, a conventional[64] line shape cannot accurately reproduce the measured spectrum,[65] resulting in a small deviation between the fit and the data. The calculated and experimental surface core-level shifts are in good agreement and are compared in Table I. The measured SCLS is consistent with previous measurements,[66] but substantially larger than the SCLS of −0.24 eV reported by Comelli *et al.*[44] The origin of this discrepancy is discussed in Ref. 66.

TABLE I. Comparison between the calculated and experimentally observed core-level shifts for the clean Pd(110) surface. The core-level shifts are referenced to the binding energy of the bulk $3d_{5/2}$ level (Pd located in the fourth layer in the calculations).

	Calculated CLS (eV)	Experimental CLS (eV)
First layer	−0.53	−0.48
Second layer	−0.07	

The surface x-ray diffraction data from the clean (1×1) surface were collected at a substrate temperature of 390 °C. Structure factors were extracted according to standard correction procedures[67] and the fit to the data was performed using the program package ROD.[68] Error bars (typically 10%) were estimated by the comparison of symmetry-equivalent reflections. The structure factors for different nonsymmetry equivalent crystal truncation rods (CTRs) are plotted together with the best fit in Fig. 2. During the fit, the topmost three layer spacings were allowed to relax, in addition to the thermal Debye-Waller (DW) factors of the layers. The bulk DW factor was fixed to $B=0.96$ Å^2.[69,70] The best fit ($\chi^2=1.7$) was achieved for an oscillatory relaxation profile and enhanced DW factors at the surface. Table II summarizes

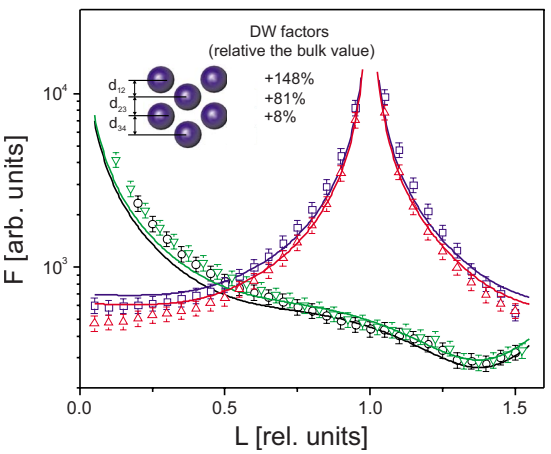

FIG. 2. (Color online) Experimental SXRD structure factors F (data points) as a function of the reciprocal lattice coordinate L perpendicular to the surface ($L=1$ corresponds to $2\pi/a_3$). Downward triangles: (−1,1) rod, circles: (−2,0) rod, squares: (−1,0) rod, and upward triangles: (0,1) rod. The solid lines represent the best fit to the data. Inset: side view of the surface along $\mathbf{a}_2$ (along the [001] direction) and definition of the relaxations. The fit result of the DW factors is included. The relaxations are discussed in the text.

TABLE II. Clean surface results of the fit to the SXRD data and comparison to the DFT results presented in this work and to literature data obtained by LEED intensity (voltage) $I(V)$ analysis. The relative interlayer distance is given in percent of the bulk distance of 1.375 Å.

	SXRD	DFT	Reference 71
d_{12} (%)	-5.7 ± 1	−9.3	-4.4 ± 1.5
d_{23} (%)	$+2.4 \pm 1$	+3.8	$+1.5 \pm 1.5$
d_{34} (%)	-0.7 ± 0.5	−0.2	

the results and also contains a comparison to literature data.

Within the error bars there is good agreement for the interlayer distances observed in the different experiments and the DFT calculations. The interlayer spacing d_{12} is contracted, whereas d_{23} is expanded. In both x-ray and DFT results a slight reduction in d_{34} is observed. The main effect of the elevated temperature during the x-ray experiment is an enhancement of the DW factor in the topmost layers. Since the relaxations agree well with calculations and LEED experiments performed at 0 K or low temperatures, we conclude that surface effects and anharmonicities in the surface atom vibrations do not play an important role for the relaxation behavior.

IV. $c(2\times4)$

A. Formation and structural model

The formation of the $c(2\times4)$ structure can be followed *in situ* using LEED. The crystal was kept at a constant temperature (300 °C) in UHV in front of the LEED optics. The oxygen pressure was then slowly increased while recording the resulting diffraction pattern. Figure 3(a) shows the diffraction pattern from the clean surface at 300 °C. As the partial oxygen pressure was slowly increased from UHV, a (1×3) structure was formed at 10^{-8} mbar, see Fig. 3(b). If the partial oxygen pressure was kept constant, the diffraction spots at $(0,\pm1/3)$ and $(0,\pm2/3)$ started to move after seven seconds [Fig. 3(c)]. After seven additional seconds, the fractional order spots stopped at $(0,\pm1/2)$, creating a (1×2) diffraction pattern which evolved during approximately half a minute to form a clear $c(2\times4)$ periodicity, as shown in Figs. 3(d) and 3(e), respectively. This seemingly smooth transformation from a (1×1) surface to $c(2\times4)$ structure, via a (1×3) and a (1×2) reconstruction, is similar to observations made in other studies.[37–39] However, the (1×3) and (1×2) phase are not studied in the present manuscript.

Previous investigations have resulted in an atomistic model for the $c(2\times4)$ structure.[48–50] This model consists of a (1×2)-missing row reconstructed surface where the remaining closed packed rows are decorated by oxygen atoms in a zigzag pattern [Fig. 4(c)]. The atomic arrangement has recently been confirmed by DFT calculations which showed that this structure is highly stable over a large pressure range.[51]

The (1×2)-missing row reconstruction is easily observed using SXRD. Figure 4(b) shows a SXRD scan along the K direction with $H=0$ and $L=0.03$. This scan is crossing the $(0,-1,L)$ rod close to the anti-Bragg position at $L=0$ and it is therefore most sensitive to the occupancy of the topmost layer. For the missing row structure every second row is missing and consequently, the diffracted intensity at $K=-1$ vanishes because of the 50% occupancy of the top layer and new reflections emerge at half integer value of K.

The results from the HRCLS measurement are presented in Fig. 4(e). The component at the lowest binding energy in the Pd $3d_{5/2}$ spectrum is assigned to the undercoordinated Pd atoms in the second layer, not bound to oxygen atoms [atoms marked with asterisk in Fig. 4(c)]. Continuing toward higher binding energy, the second peak originates from emission from the Pd bulk, whereas the third and fourth components correspond to Pd atoms coordinated to one and two oxygen atoms, respectively. The calculated and experimentally observed core-level shifts (CLSs) for the Pd $3d_{5/2}$ are in excellent agreement and are presented in Table III. These CLS differ from those reported by Comelli *et al.*[44] This discrepancy can be explained by the much lower resolution of the spectrum in Ref. 44, and a decomposition based on a model proposed by Jo *et al.*,[38] which does not include a (1×2)-missing row reconstruction or Pd atoms coordinated to two oxygen atoms. According to the structural model in Fig. 4(c) the intensity ratio between the three shifted components in the $3d_{5/2}$ spectrum should be 1:1:1. The intensity ratio between the components from the second layer (+0.44 and −0.45 eV) is indeed close to 1:1. However, the intensity from the topmost layer (+0.59 eV) is approximately a factor of five higher. We attribute the discrepancy in the intensities between the first and second layers to attenuation of the photoemitted electrons and to diffraction effects, which at these relative low kinetic energies may result in substantial intensity errors. The spectrum from the O 1*s* level is shown in Fig. 4(e), which is fitted with one component in accordance with the model.

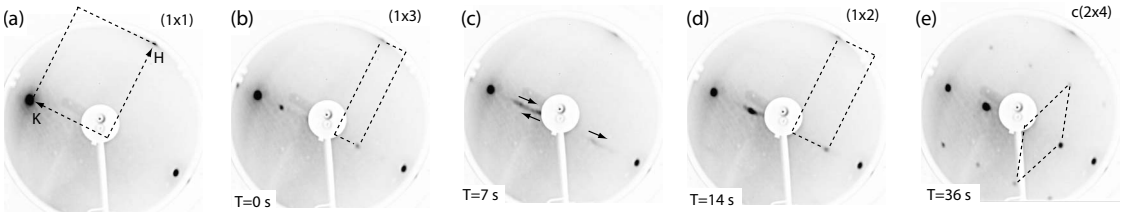

FIG. 3. *In situ* LEED experiment at constant temperature (300 °C). (a) Clean surface. (b) At an oxygen pressure of 10^{-8} mbar, a (1×3) structure is formed. (c) After seven seconds the fractional order diffraction spots starts to move, (d) resulting in a (1×2) structure, and (e) finally a $c(2\times4)$.

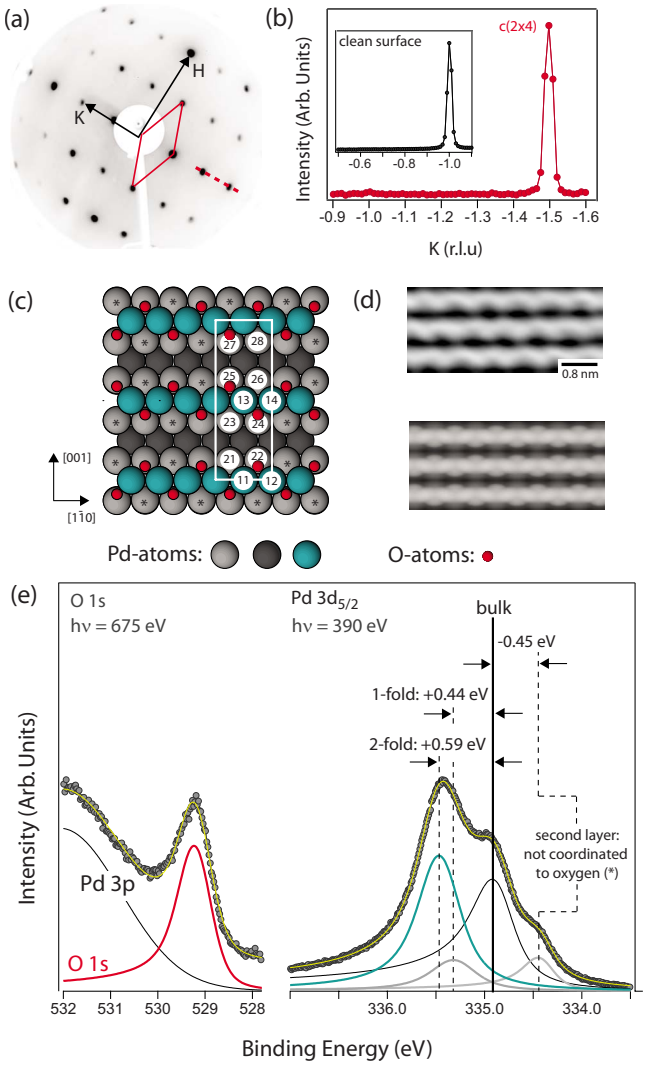

FIG. 4. (Color online) (a) LEED pattern from the $c(2\times4)$ structure. (b) SXRD scan along the broken line in (a) ($H=0$ and $L=0.03$) Inset: the clean surface. (c) Atomic model of the $c(2\times4)$ structure as calculated by DFT. Large and small spheres corresponds to Pd and O atoms, respectively. (d) Top: experimental STM image ($U=0.1$ V and $I=1.5$ nA) Bottom: simulated STM image of the $c(2\times4)$ structure. (e) HRCLS from a preparation resulting in a $c(2\times4)$ LEED pattern.

TABLE III. Comparison between the calculated and experimentally observed core-level shifts in the $c(2\times4)$ structure. The core-level shifts are referenced to the binding energy of the bulk $3d_{5/2}$ level (Pd located in the fourth layer in the calculations). The assignment of numbers to the different atoms can be inferred from Fig. 4(c).

$c(2\times4)$	Calculated CLS (eV)	Experimental CLS (eV)
$Pd_{11\rightarrow14}$	0.59	0.59
$Pd_{21,26}$	−0.40	−0.45
$Pd_{22,25}$	0.45	0.44
$Pd_{23,28}$	−041	−0.45
$Pd_{24,27}$	0.44	0.44

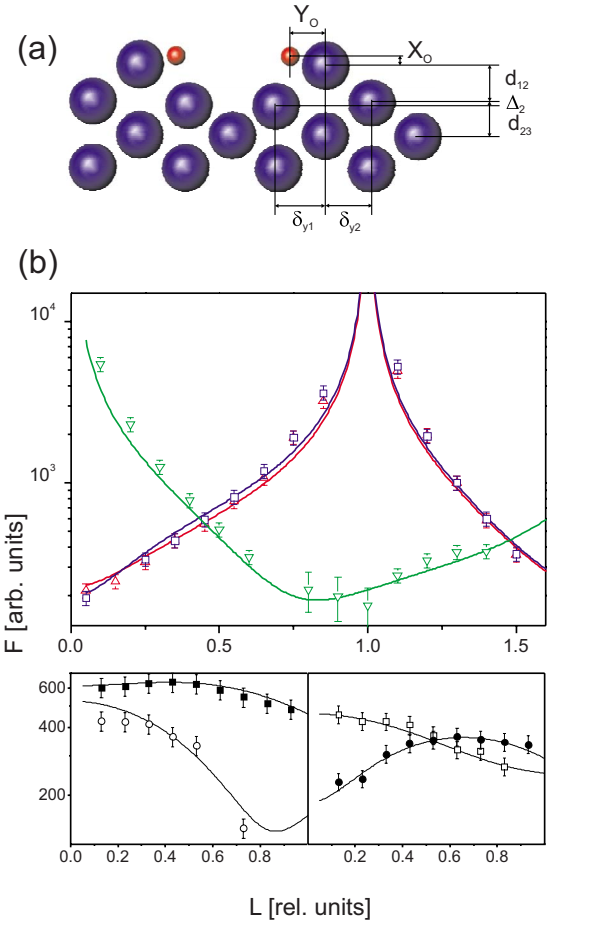

FIG. 5. (Color online) (a) Oxygen-induced $c(2\times4)$ reconstruction projected along $\mathbf{a}_1$ (along the $[1\bar{1}0]$ direction). Small spheres represent oxygen atoms, large spheres Pd atoms. The relaxation parameters are indicated and reported in Table III. (b) Structure factors of the $c(2\times4)$ reconstructed surface (data points) and best fit (solid lines). Upper panel: CTRs (downward triangles: (1,−1) rod, squares: (0,1) rod, and upward triangles: (1,0) rod). Lower panel: surface rods: (open circles: (0,−3/2) rod, filled squares: (0,1/2) rod, open squares: (1,−1/2) rod, and filled circles: (1,−3/2) rod.)

The x-ray diffraction experiment for quantitative determination of the structure was performed *in situ* at an oxygen pressure of 8×10^{-8} mbar and a sample temperature of 430 °C. Note, that at 430 °C, the oxygen induced $c(2\times4)$ reconstruction is not stable under UHV conditions. In Fig. 5(a) a side view of the structure is given, together with the relaxation parameters used for the fit. Relaxations were allowed according to the internal symmetry of the $c(2\times4)$ structure. In Fig. 5(b) the x-ray data and the fit are presented.

Table IV summarizes the best-fit results and compares them to the DFT results presented in this study and the LEED I(V) results from Ref. 43. The best fit was achieved with enhanced DW factors (from the topmost layer): B1 =9.4 Å^2, B2=4.7 Å^2, and B3=1.3 Å^2, with bulk DW factor of 1.01 Å^2 at 430 °C. The enhanced DW factors may be the result of the lower coordination of the surface atoms taking part in the reconstruction or strain which is built up during the formation of large $c(4\times2)$ domains. In the fol-

TABLE IV. Best-fit ($\chi^2=1.7$) displacement parameters compared to DFT values and LEED $I(V)$ results from Ref. 43. The z displacements are given in % of the interlayer (220) spacing of 1.375 Å the y displacements in % of the interlayer (002) spacing of 1.945 Å. The distance of the oxygen atoms relative to the Pd atoms was kept at the DFT values, since the x-ray fit turned out to be not very sensitive to the position of the oxygen atoms. An occupancy of 85% was obtained from the fit for the surface Pd atoms in the missing row structure.

	X-ray	DFT	Reference 43
d_{12} (%)	$+9.8\pm2$	+18.3	$+0.4\pm2.2$
d_{23} (%)	$+4.2\pm1$	−3	-4.7 ± 2.2
d_{34} (%)	-0.6 ± 0.5	+1.2	
Δ_2 (%)	$+12.2\pm2.4$	+4.4	-5.8 ± 3.6
X_O (Å)	0.156	+0.156	0.31 ± 0.02
δ_{y1} (%)	$+6.4\pm1.3$	+2.7	$+4.3\pm8.2$
δ_{y2} (%)	0 ± 1.3	−2.1	$+1.3\pm5.8$
Y_O (Å)	1.375	1.375	$(+1.21\pm0.16)$

lowing we will briefly discuss the main differences/similarities of the results obtained by the different techniques. Most prominently, both x-ray and the DFT results show that the Pd atoms of the reconstructed rows exhibit a strong outward relaxation ($d_{12}=10-18$ %), which is not observed in the LEED study. This strong outward relaxation is also in line with an EELS study of the location of the oxygen atoms within the $c(2\times4)$ structure.[49] A second remarkable point is the buckling of the first substrate layer (represented by parameter Δ_2). Both x-ray diffraction and DFT find that the Pd atoms sitting nearly below the oxygen atoms [atoms 22, 24, 25, and 27 in Fig. 4(c)] move downward compared to the Pd atoms in the first substrate layer without oxygen nearest neighbor [atoms 21, 23, 26, 28 in Fig. 4(c)]. This behavior is opposite in the LEED study, e.g., first substrate-layer Pd atoms close to oxygens move up. In all three studies it is found that the first substrate-layer Pd atoms close to oxygen atoms are laterally displaced in the direction of the troughs (δ_{y1}, δ_{y2}). The x-ray diffraction and DFT results differ in the sign of d_{23}, the first and second substrate interlayer spacing. To test the significance of this difference we have fitted d_{23} using the DFT model and the DW factors and surface occupancy from our best fit. As a result, we find that the fit improves significantly for an increased layer spacing. A possible explanation for this difference could be the role of the elevated temperature and oxygen atmosphere, resulting in a high vibrational amplitude of the surface atoms, which may give rise to a different relaxation behavior as compared to 0 K. Finally, the oxygen bonding geometry differs slightly for the DFT and the LEED study. In DFT it is found that oxygen sits on highly symmetric sites with a distance of 1.95 Å to all three nearest-neighbor Pd atoms, whereas in the LEED study the bond distance is shorter and asymmetric (1.85 Å to the nearest-neighbor substrate atom and 1.88 Å to the row atoms).

B. Antiphase domain boundaries

Figure 6(a) shows a large scale STM image recorded after a preparation resulting in a $c(2\times4)$ LEED pattern. The STM image shows a surface which is covered by bright strips in the $[1\bar{1}0]$ direction. Zooming in on these bright stripes shows that an atomic row has been added, locally lifting the missing row reconstruction [Fig. 6(b) (top)]. As a result, two domains of the $c(2\times4)$ structure on opposite side of these "double" rows are out of phase with respect to each other. This is illustrated in Fig. 6(c) where lines with a (1×2) periodicity have been added on top of the STM image. The lines are positioned on top of the close-packed rows on the left side of the image, however, after crossing the double row, the lines are instead positioned at the missing rows. Adding rows thus results in antiphase domain walls, separating the $c(2\times4)$ domains. A model of the situation is shown in Figs. 6(d) and 6(e), where we assume that the oxygen atoms occupy the same sites at the antiphase domain boundaries as in the $c(2\times4)$ structure.

C. Evolution of the $c(2\times4)$ structure

At this stage, we will continue to discuss the LEED experiment described in Sec. IV A and Fig. 3, now concentrat-

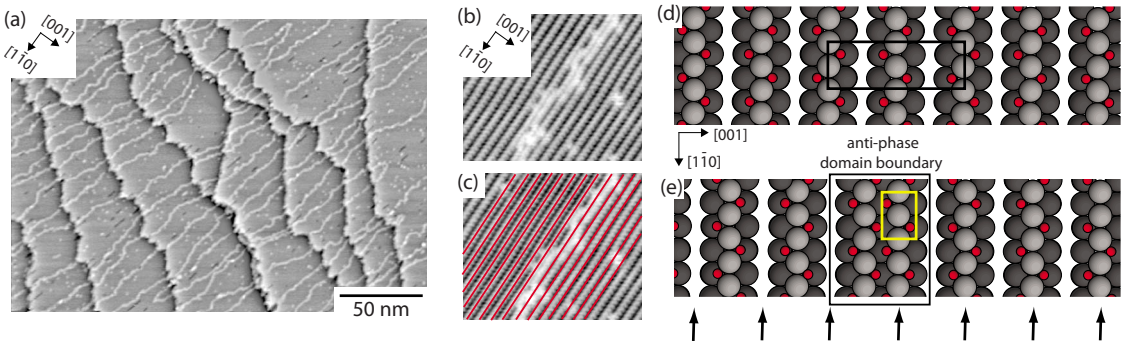

FIG. 6. (Color online) (a) STM image from a preparation yielding a $c(2\times4)$ LEED pattern. The surface exhibits bright stripes along the $[1\bar{1}0]$ direction which are separated by approximately 5–25 nm in the [001] direction ($U=0.1$ V and $I=1.5$ nA). (b) Zoom in on one of the bright stripes in (a) ($U=0.1$ V and $I=1.5$ nA). (c) By adding lines with a (1×2) periodicity, one can see that the double rows constitutes antiphase domain boundaries. (d) Model of the $c(2\times4)$ structure structure. (e) Model of a situation where one row has been added. The oxygen atoms are assumed to occupy the same sites on the antiphase domain boundary as in the $c(2\times4)$, thereby creating a local $(2\times1)-2O$ structure (yellow unit cell).

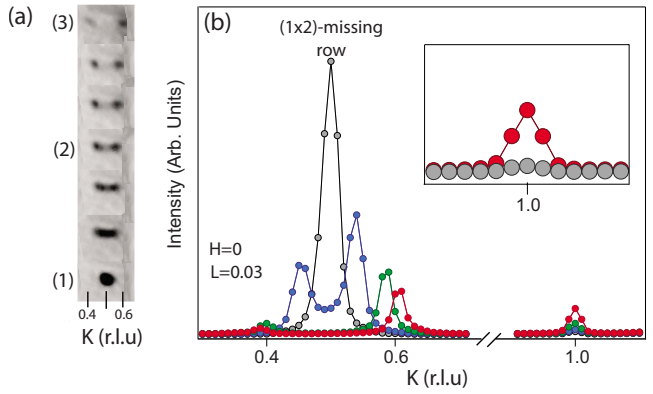

FIG. 7. (Color online) (a) LEED and (b) SXRD at $L=0.03$. Evolution of the (0,0.5) diffraction spot over a time period of four minutes at 10^{-6} mbar of oxygen at 300 °C.

ing solely on the half order diffraction spot at (0,0.5) [Fig. 7(a)]. As the oxygen pressure is increased to 10^{-6} mbar the half order spot (0,0.5) starts to split, see Fig. 7(a). Keeping the oxygen pressure (10^{-6} mbar) and the temperature (300 °C) constant, the splitting increases gradually with time, resulting in two diffraction spots at approximately $K=0.4$ and 0.6 after roughly four minutes. The same experiment can be performed using *in situ* SXRD and the results are shown in Fig. 7(b). Here we have also observed that the splitting can continue beyond $K=0.6$ with heavily reduced intensity of the diffraction peaks. Note that the intensity of the diffraction signal at $K=1$ increases as the magnitude of the split becomes larger.

Using STM the diffraction data can be explained. Figures 8(a) and 8(b) shows STM images taken after two different preparations, resulting in a split of the half order diffraction spot corresponding to (2)–(3) in Fig. 7(a). One can see that the average distance between the antiphase domain boundaries becomes smaller as the magnitude of the split increases. As a consequence, the domains of the $c(2\times4)$ quickly becomes very small, which explains the disappearance of the diffracted intensity at $K=0.5$. The detected intensity corresponds now to the statical distribution of the distance between the domain walls.[72–74] A previously reported (2×3)-1D structure[46] could be a consequence of antiphase domain boundary formation, all though we have not observed this structure during our investigations.

When the split of the half order diffraction signal has reached approximately $K=0.6$ and 0.2, most of the missing rows are filled [Fig. 8(b)]. This results in a (1×1) like surface, explaining the reappearance of the diffraction signal at $K=1$. By closely examining the STM image in Fig. 8(b) one can see areas with small bright elongated features appearing where two (or more) neighboring missing rows have been filled.

Increasing the oxygen pressure to 5×10^{-6} mbar results in the surface shown in Fig. 8(c). Here almost every missing row is filled, resulting in a surface which is covered with more or less ordered arrays of bright elongated features.

V. "COMPLEX STRUCTURE"

As the oxygen exposure is increased to 10^{-5} mbar, all missing rows are filled, and the bright features have now

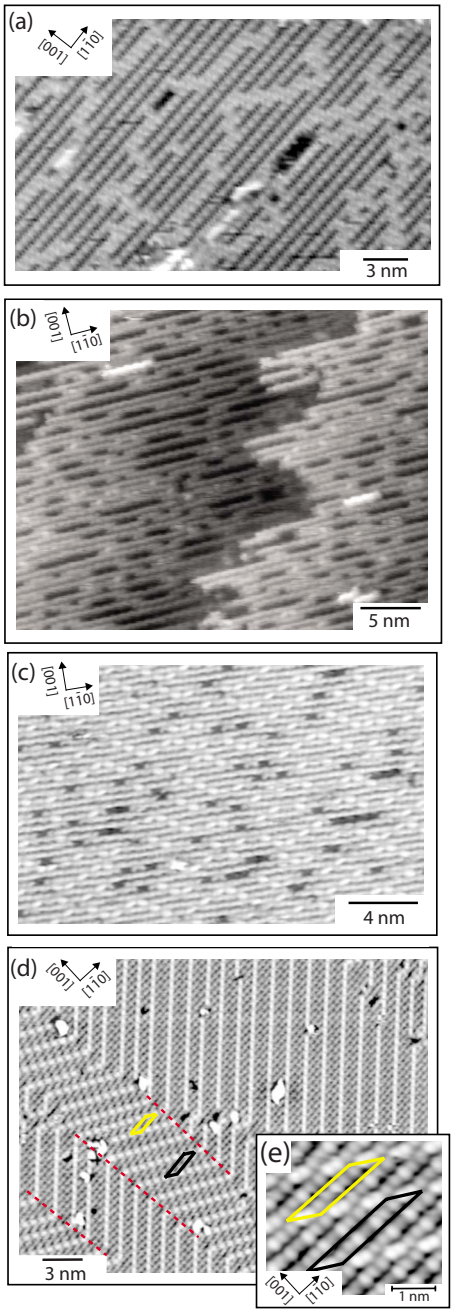

FIG. 8. (Color online) [(a)–(b)] STM images recorded after a preparation yielding a LEED pattern with a split of the (0,0.5) spot corresponding to (2)–(3) in Fig. 7(a) [$U=-0.05(-0.1)$ V and $I=1.5(0.4)$ nA], respectively. (c) The Pd(110) surface after oxygen exposure in the pressure range $5\times10^{-6}-10^{-5}$ mbar and a sample temperature of 300 °C ($U=-0.3$ V $I=0.1$ nA). [(d)–(e)] The complex structure ($U=0.01$ V and $I=0.5$ nA).

arranged themselves to form highly ordered domains of the complex structure, also denoted as $(7\times\sqrt{3})$ and $(9\times\sqrt{3})$,[52] see Fig. 8(d) and Figs. 9(a) and 9(b). As can be seen from the STM image in Fig. 8(e), the elongated features in Figs. 8(b)–8(d) are pairs of Pd atoms which are displaced from their (1×1) surface positions along the [001] direction. The reason for these rather large displacements are summarized in Fig. 9(b), and discussed in detail in Ref. 52. By filling the

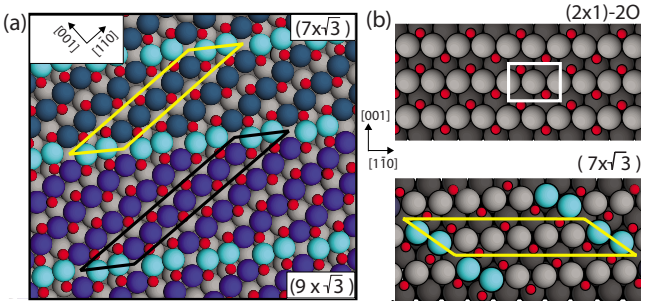

FIG. 9. (Color online) (a) Model of the complex structure. (b) An oxygen coverage of 1ML could be obtained by forming a $(2\times1)-2O$ structure. However, this structure induces a large compressive stress along the [001] direction. This stress is relieved by displacing pairs of Pd atoms at the end of chains containing 7 (or 9, not shown) atoms in the $[1\bar{1}0]$ direction.

missing rows, assuming that the oxygen atoms occupy the same sites as in the $c(2\times4)$ [Figs. 6(d) and 6(e)], the surface will eventually be covered with a $(2\times1)-2O$ structure, see Fig. 9(b). This structure is, however, energetically unfavorable due to the short O-O distance which induces a large compressive stress between the Pd rows along the [100] direction. However, by forming the $(7\times\sqrt{3})$ and $(9\times\sqrt{3})$ structures, most of the surface stress is relieved, which stabilizes the structure.[52]

VI. OXIDE FORMATION

Previous studies have shown that the $(7\times\sqrt{3})$ and $(9\times\sqrt{3})$ structures form if the crystal is exposed to oxygen pressures between 10^{-5} and 5×10^{-3} mbar at sample temperatures 250–350 °C.[52] Both the Pd(111) and the Pd(100) form thin well-ordered surface oxides in this pressure range.[14,15] A natural assumption would be that a surface oxide would also form on the Pd(110) surface, as the case is for the Rh(110) surface.[24] We therefore performed additional experiments at elevated oxygen pressures.

If the oxygen pressure is increased above 10^{-2} mbar at a sample temperature of 350 °C, new diffraction peaks starts to appear at $(0,\pm1.45,0.03)$ and (0.92, 0.03). As the peak at (0, 1.45, 0.03) continues to grow with increasing oxygen pressure, the diffraction signal from the clean surface decreases, see Fig. 10(a). Between 5×10^{-1} and 50 mbar of oxygen the intensity of the fractional peak stays constant whereas the signal from the surface disappears. Since the new reflections are present at high oxygen pressures they most likely originate from the PdO bulk oxide. Figure 10(b) shows a HRCL spectrum from the Pd $3d_{5/2}$ region after exposing the crystal to 5×10^{-3} mbar of O_2 at a sample temperature of 300 °C, which is close to the lower limit where we suspect that PdO forms. The spectrum can be decomposed into five components, where the first three peaks at higher binding energy (blue) than the bulk peak, can be assigned to Pd atoms participating in the complex structure as described in Ref. 52. However, the fourth component at the highest binding energy (336.2 eV, red) cannot be explained by the model for the complex structure. This peak exhibits an

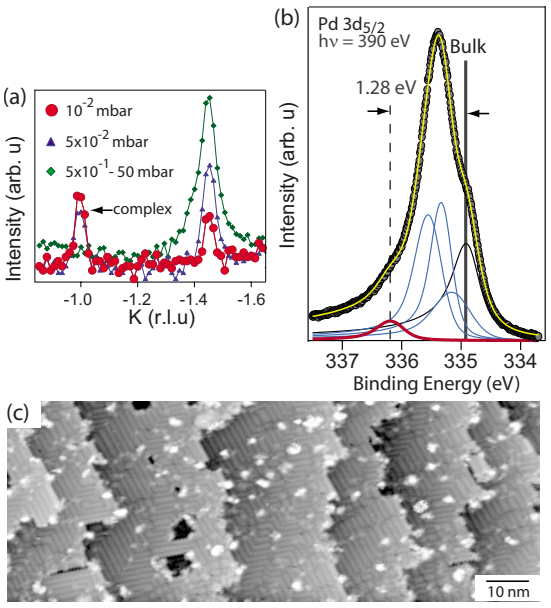

FIG. 10. (Color online) SXRD scan along K with $H=0$ and $L=0.03$, i.e., along the [001] direction. (b) HRCL spectrum taken after exposing the crystal to 5×10^{-3} mbar of oxygen at 300 °C. (c) STM images taken after a similar preparation as in (b) ($I=0.05$ nA and $U=2$ V).

energy shift of 1.28 eV which is characteristic for Pd atoms coordinated to four oxygen atoms.[14,15,33] The STM images in Figs. 10(c) and 10(d) where taken after a preparation similar to the preparation resulting in the HRCL spectrum in Fig. 10(b). The resulting LEED image (not shown) displayed a weak, not well-defined diffraction pattern from the complex structure. By inspection, one can see that the surface in Fig. 10(d) exhibit the characteristic domains of the complex "structure" [bright lines, compare with Fig. 8(d)]. Although the domains are still quite well ordered in this STM image, much of the surface displays highly unordered and disrupted domains as shown in Fig. 10(c). Furthermore, the surface is also covered with white protrusions. These protrusions were also present in the STM images taken at a lower O_2 pressures [Fig. 8(d)], but not to the same extent. As discussed previously in this section, the SXRD measurements indicate that we form bulk PdO at oxygen pressures between $10^{-2}-100$ mbar. Since the experiment was performed close to the lower limit of this pressure range when preparing the surface for the STM measurements presented in Fig. 10, we believe that the protrusions covering the surface in these STM images are small clusters of PdO, similar to on Pd(100) at oxygen coverage above the $(\sqrt{5}\times\sqrt{5})$, using NO_2.[75] This would also explain the presence of a component with a binding energy shift of 1.28 eV in the HRCL spectrum.

We now continue to investigate the surface at oxygen pressures between $10^{-2}-100$ mbar. Due to the high partial pressures involved, we now solely turn to *in situ* SXRD. In a first attempt we performed out-of-plane scans (along L) at the positions for the suspected PdO reflections at $(0,\pm1.45,0.03)$ and $(\pm0.92,0.03)$. No sharp peaks were detected with increasing L as would be expected for bulk oxide. In order to refine the out-of-plane position of the bulk reflec-

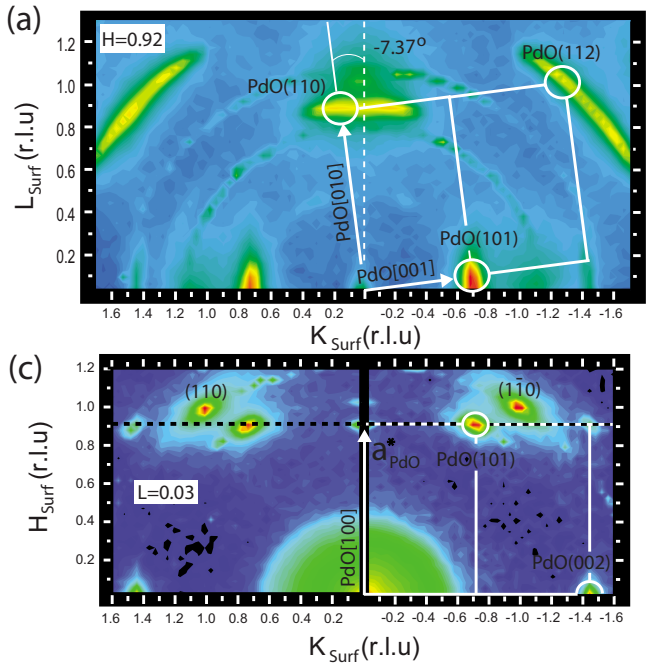

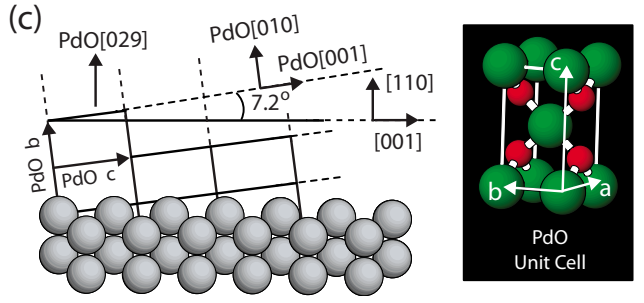

FIG. 11. (Color online) Detected diffraction intensity in planes perpendicular (a), and parallel (L=0.03) (b), to the Pd(110) surface. High and low intensity is indicated as red and blue, respectively. The HL plane in (a) is cutting the HK plane along the dotted line $(0.92, K)$ in (b). All the detected intensity at fractional values of H, K, and L, can be related to planes in the PdO bulk oxide. The reciprocal PdO lattice vectors, b^* (parallel to PdO[010]), and c^* (parallel to PdO[001]), are rotated $\pm 7.34°$ with respect to the surface normal and the HK plane, respectively, see (a). The reciprocal PdO sublattice, here rotated $-7.34°$, is indicated in (a) and (b) with white lines. Here the Pd sublattice is described as body-centered tetragonal, resulting in strong Bragg reflections (indicated by white circles), only when the sum of the indices is even or odd. A possible orientation for the PdO growth, as determined from the diffraction data in (a) and (b), is shown in (c).

tions, as well as to map out the in-plane periodicity of the oxide structure, mesh scans were performed along planes perpendicular and parallel to the surface. Figures 11(a) and 11(b) show the resulting intensity distribution in the KL plane (H=0.92) and the HK plane (L=0.03), respectively. The KL mesh now reveals bulk reflections located at $L \sim 0.9$. Looking at Fig. 11(a) one can clearly see that the $(0.92, 0, L)$ rod is split into two CTRs which are tilted with respect to the surface normal. In fact, all detected reflections can be assigned to atomic planes in the PdO bulk oxide, and the reciprocal PdO lattice is shown together with the mesh

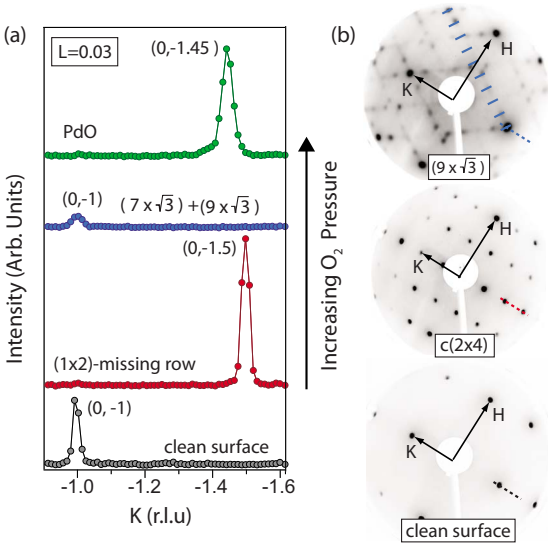

FIG. 12. (Color online) (a) SXRD scans along the negative K direction (with H=0, i.e., perpendicular to the closed packed rows, at L=0.03. (b) LEED pattern corresponding to the clean surface, the $c(2\times4)$, and the $(9\times\sqrt{3})$ structure. The broken line in the LEED images corresponds (in plane) to the SXRD scans in (a).

scans in Figs. 11(a) and 11(b). Although the mesh scans show powder rings from the PdO, there are well defined PdO Bragg reflections, indicating that there is a preferable orientation in which the bulk oxide grows. The angle at which the PdO rods are tilted ($\pm 7.37°$) is close to the angle between the PdO(029) plane and the Pd(110) surface ($\pm 7.2°$). A possible orientation in which the PdO grows with respect to the substrate is with the a side along the closed packed row and the c and b axes rotated ($\pm 7.2°$) with respect to the [010] and [110] directions of the substrate, respectively, see Fig. 11(c).

As mentioned above, detecting the PdO throughout this large pressure range clearly differs from our previous investigation of low index and vicinal Pd surfaces. In the case of the Pd(100), Pd(111), and Pd(553) a thin surface oxide forms prior to the formation of a thicker bulk oxide.[14,15,22]

VII. PHASE DIAGRAM

Using SXRD we can identify the different phases present on the surface *in situ*. By scanning along the K direction with H=0, we are detecting diffracted intensity corresponding to the periodicity perpendicular to the closed packed rows, i.e., along the [001] direction. Furthermore, by performing this scan at an L value close to the minimum of the CTR at L =0, we only probe the topmost atomic layer. The result from the SXRD experiment and selected LEED images are presented in Figs. 12(a) and 12(b), respectively. Starting at UHV with a (1×1) surface and increasing the oxygen pressure stepwise, keeping the temperature constant, resulted in a a diffraction peak at $(0,-1.5)$. This reflection originates from the (1×2) missing row reconstruction, and thus, indicates the presence of the $c(2\times4)$ structure. For the same reason, the previously detected peak at $K=-1$ has now disappeared.

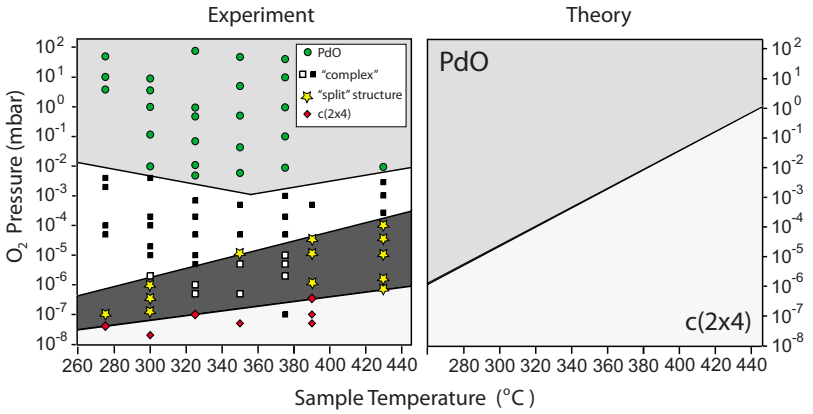

FIG. 13. (Color online) (a) Experimental (T,p) diagram obtained by performing the K scan in Fig. 12(a) at different partial oxygen pressures and sample temperatures. The dark gray area (bottom) corresponds to the $c(2\times4)$ structure, the white area to the $(7\times\sqrt{3})$ and $(9\times\sqrt{3})$ structures, and the light gray (top) is the PdO bulk oxide. The "split structure" (denoted by a star) refers to the situation in Fig. 8(b), where diffraction intensity is detected at approximately $K=-1.4$ and -1.6. (b) Theoretical surface phase diagram, displaying the thermodynamically stable phases as calculated by DFT.

As the oxygen pressure was increased, the half order peak started to split (not shown, see Fig. 7) and a small signal reappears at $(0,-1)$. By increasing the pressure even further, the splitting will disappear, and the only remaining intensity is detected at $K=-1$. The reappearance of the peak at integer value is assigned to the formation of the $(7\times\sqrt{3})$ and $(9\times\sqrt{3})$ structures and the formation of a (1×1)-like surface. This is, however, only an indirect proof for the presence of these two structures. Nevertheless, since we know from the HRCLS, STM, and LEED measurements that the $(7\times\sqrt{3})$ and $(9\times\sqrt{3})$ structures are formed at these pressures and temperatures, we are confident that the reappearance of the peak at $(0,-1)$ can be used to identify this phase. Furthermore, all other reported oxygen-induced structures on Pd(110) involves some kind of missing-row reconstruction, which consequently would result in diffraction peaks at fractional values of K. When the oxygen pressure reaches approximately 10^{-2} mbar, reflections corresponding to PdO appear and the signal at $(-1,0)$ starts to decrease.

Having established the means to distinguish the different structures *in situ*, we can obtain a stability diagram by performing the scan presented in Fig. 12(a) at different partial oxygen pressures and sample temperatures, see Fig. 13(a). The thermodynamically most stable phases at the experimental conditions were calculated using DFT, and the resulting theoretical phase diagram is shown in Fig. 13(a). A closer inspection of the PdO formation reveals deviations between experiment and theory. According to theory the bulk oxide should form at decreasing oxygen pressures as the sample temperature is lowered. Experiment shows the same behavior in the high temperature region of the (T,p) diagram, but, as the sample temperature is lowered below ~350 °C, an inverse behavior is observed. Since the DFT calculations determine the most stable phase at the thermodynamic equilibrium between surface and gas phase, we attribute the discrepancies between theory and experiment to kinetic limitations for the growth of the bulk oxide under these conditions.

Neglected in these calculations are the mirror domains (red dotted lines in Fig. 8) that always forms together with the $(7\times\sqrt{3})$ and $(9\times\sqrt{3})$ structures. The formation of these mirror domains results in an energy gain, which most likely makes these two structures the most energetically favorable phase under certain (T,p) conditions.[52] Also excluded from the calculations is the evolution of the $c(2\times4)$ structure, as described in Sec. IV C. The situation in Fig. 8(b) is denoted by a star in the experimental (T,p) diagram (the "split structure").

VIII. DISCUSSION

The most surprising observation in the O/Pd(110) system is that no surface oxide is observed, in contrast to what has been observed on the previously investigated Pd(111), Pd(100), and Pd(553) surfaces.[14,15,22] Instead, the PdO bulk oxide is formed directly from a structure induced by chemisorbed oxygen, namely the complex structure. The fact that no surface oxide forms on the Pd(110) surface explains the early formation of the bulk oxide reported in the present manuscript. For both the Pd(100) and the Pd(111) surfaces the thin surface oxide prevents further oxidation,[25] resulting in PdO formation only at higher values of the chemical potential than predicted by theory [around 300 °C at an oxygen pressure of 2–10 mbar for both Pd(100) and Pd(111)]. We conclude that surface oxide layers on other low-index surfaces present significant kinetic barriers for bulk oxide formation.

The absence of a thin oxide in the Pd(110) case can most likely be explained by the already high oxygen coverage for the complex $(7\times\sqrt{3})$ and $(9\times\sqrt{3})$ structures (0.86 and 0.89 ML,[52] respectively), as compared to the surface oxides on the Pd(100) and Pd(111) surfaces [0.8 ML (Ref. 15) and 0.69 ML,[14] respectively]. Kinetic barriers appear to be much lower for the more open Pd(110) surface, on which a more facile mass transport is possible.

All experimental data for the O/Pd(110) system shown in the present manuscript can be explained by either chemisorbed oxygen or the formation of bulk PdO, in agreement with previous measurements of this surface.[53] Therefore, early models using subsurface oxygen as an active species in for example CO oxidation can be excluded.[76]

Facile oxide formation could very well be of importance in catalysis, both for single crystal model surfaces and nm sized particles. As described above, a recent *in situ* STM CO oxidation experiment on Pd(100) using ambient pressures at 135 °C, Hendriksen and Frenken[4] concluded that on a Pd(100) surface, the appearance of a rough but thin bulk PdO film, resulted in a significant increase in the CO_2 production. Similar observations have been made using *in situ* SXRD,[12,13] using both a batch reactor and a micro-flow reactor. If PdO formation on Pd promotes catalytic oxidation

reactions, facile PdO formation would be beneficial for the reaction rate, and the Pd(110) would be a highly active Pd surface due to the early bulk oxide formation, as compared to Pd(100) and (111).

On the other hand, the situation could also be reversed. In a set of recent articles, Goodman and co-workers[7–10] have investigated the CO oxidation on Pd by the use of PM-IRAS and *ex situ* XPS, in order to determine the active phase. Surprisingly, these workers could not identify any oxide as being an active phase. It was reported that for Pd(100) a "hyperactive" phase exists, which had an oxygen coverage of approximately 1 ML (Ref. 7) based on *ex situ* XPS, and it was concluded in the most recent report that the hyperactive phase was rather due to chemisorbed oxygen,[8–10] and that oxide formation poisons the reaction. A chemisorbed oxygen phase with a coverage of 1 ML has only been reported by these authors for this surface. In this case the early oxide formation on Pd(110) would inhibit the CO_2 formation at lower pressures than Pd(100) and Pd(111), if the formation of surface oxides are ignored.

In addition to chemisorbed oxygen structures and PdO formation on Pd surfaces, surface oxides are also present on the Pd(100) and Pd(111) surfaces. Indeed, in a recent theoretical paper, Rogal *et al.*[5] suggested that in conditions representative of technological CO oxidation catalysis, the surface oxide on Pd(100)[5] could actually be an highly active phase. No experimental information on the activity of the surface oxide on Pd(100) or Pd(111) exists, but if the surface oxides forming at oxygen partial pressures of 10^{-6}–10^{-3} mbar 300 °C on Pd(100) and Pd(111) are as active as the bulk PdO, the Pd(110) would be an in comparison poor surface for CO oxidation catalysis, since no surface oxide or bulk oxide exists at these pressures on the (110) surface.

IX. SUMMARY

We have studied the oxidation of the Pd(110) surface at an oxygen pressure of 10^{8}–100 mbar by LEED, STM, HRCLS, SXRD, and DFT. From this data we have constructed an *in situ* stability diagram in the temperature range 260–440 °C. At low partial oxygen pressures (10^{-8} mbar) we detect a $p(1\times3)$ LEED pattern which rapidly ($t<60$ s) transforms into structures with a $p(1\times2)$ and $c(2\times4)$ periodicity. Since the $p(1\times3)$ and $p(1\times2)$ structures are not stable during in *in situ* conditions, we are here focused on the $c(2\times4)$ structure which transforms via the formation of antiphase domain walls into a complex structure denoted as $(7\times\sqrt{3})/(9\times\sqrt{3})$. Contrary to what have been observed on other Pd surfaces,[14,15,22] we do not detect any evidence for the existence of an ordered two dimensional surface oxide, instead we observe an early formation ($\sim10^{2}$ mbar) of the PdO bulk oxide. The facile oxide formation on the Pd(110) surface is discussed in the context of the catalytic CO oxidation over Pd surfaces.

ACKNOWLEDGMENTS

This work was financially supported by the Swedish Research Council, the Crafoord Foundation, the Knut and Alice Wallenberg Foundation, the Anna and Edwin Berger Foundation, and the Austrian Fonds zur Förderung der wissenschaftlichen Forschung (FWF).

[1] H. S. Gandhi, G. W. Graham, and R. W. McCabe, J. Catal. **216**, 433 (2003).
[2] A. Stierle and A. Moelenbroek, MRS Bull. **32**, 1000 (2007).
[3] E. Lundgren and H. Over, J. Phys.: Condens. Matter **20**, 180302 (2008).
[4] B. L. M. Hendriksen and J. W. M. Frenken, Surf. Sci. **552**, 229 (2004).
[5] J. Rogal, K. Reuter, and M. Scheffler, Phys. Rev. Lett. **98**, 046101 (2007).
[6] G. Rupprechter and C. Weilach, NanoToday **2**, 20 (2007).
[7] M. S. Chen, Y. Cai, Z. Yan, K. K. Gath, S. Axnanda, and D. W. Goodman, Surf. Sci. **601**, 5326 (2007).
[8] F. Gao, Y. Wang, Y. Cai, and D. W. Goodman, J. Phys. Chem. C **113**, 174 (2009).
[9] F. Gao, S. M. McClure, Y. Cai, K. K. Gath, Y. Wang, M. S. Chen, Q. L. Guo, and D. W. Goodman, Surf. Sci. **603**, 65 (2009).
[10] S. M. McClure and D. W. Goodman, Chem. Phys. Lett. **469**, 1 (2009).
[11] F. Gao, M. Lundwall, and D. W. Goodman, J. Phys. Chem. C **112**, 6057 (2008).
[12] M. D. Ackermann, Ph.D. thesis, Leiden University, 2007.
[13] R. van Rijn, O. Balmes, R. Felici, J. Gustafson, D. Wermeille, R. Westerström, E. Lundgren, and J. W. M. Frenken (unpublished).
[14] E. Lundgren, G. Kresse, C. Klein, M. Borg, J. N. Andersen, M. De Santis, Y. Gauthier, C. Konvicka, M. Schmid, and P. Varga, Phys. Rev. Lett. **88**, 246103 (2002).
[15] M. Todorova, E. Lundgren, V. Blum, A. Mikkelsen, S. Gray, J. Gustafson, M. Borg, J. Rogal, K. Reuter, J. N. Andersen, and M. Scheffler, Surf. Sci. **541**, 101 (2003).
[16] W. X. Li, L. Österlund, E. K. Vestergaard, R. T. Vang, J. Matthiesen, T. M. Pedersen, E. Lægsgaard, B. Hammer, and F. Besenbacher, Phys. Rev. Lett. **93**, 146104 (2004).
[17] J. Gustafson, A. Mikkelsen, M. Borg, E. Lundgren, L. Köhler, G. Kresse, M. Schmid, P. Varga, J. Yuhara, X. Torrelles, C. Quiros, and J. N. Andersen, Phys. Rev. Lett. **92**, 126102 (2004).
[18] J. Gustafson, A. Mikkelsen, M. Borg, J. N. Andersen, E. Lundgren, C. Klein, W. Hofer, M. Schmid, P. Varga, L. Köhler, G. Kresse, N. Kasper, A. Stierle, and H. Dosch, Phys. Rev. B **71**, 115442 (2005).
[19] J. Gustafson, A. Resta, A. Mikkelsen, R. Westerström, J. N. Andersen, E. Lundgren, J. Weissenrieder, M. Schmid, P. Varga, N. Kasper, X. Torrelles, S. Ferrer, F. Mittendorfer, and G. Kresse, Phys. Rev. B **74**, 035401 (2006).
[20] E. Lundgren, A. Mikkelsen, J. N. Andersen, G. Kresse, M. Schmid, and P. Varga, J. Phys.: Condens. Matter **18**, R481 (2006).
[21] P. Kostelnik, N. Seriani, G. Kresse, A. Mikkelsen, E. Lundgren,

V. Blum, T. Sikola, P. Varga, and M. Schmid, Surf. Sci. **601**, 1574 (2007).
[22] R. Westerström, J. Gustafson, A. Resta, A. Mikkelsen, J. N. Andersen, E. Lundgren, N. Seriani, F. Mittendorfer, M. Schmid, J. Klikovits, P. Varga, M. D. Ackermann, J. W. M. Frenken, N. Kasper, and A. Stierle, Phys. Rev. B **76**, 155410 (2007).
[23] H. H. Kan and J. F. Weaver, Surf. Sci. **602**, L53 (2008).
[24] C. Dri, C. Africh, F. Esch, G. Comelli, O. Dubay, L. Köhler, F. Mittendorfer, G. Kresse, P. Dudin, and M. Kiskinova, J. Chem. Phys. **125**, 094701 (2006).
[25] E. Lundgren, J. Gustafson, A. Mikkelsen, J. N. Andersen, A. Stierle, H. Dosch, M. Todorova, J. Rogal, K. Reuter, and M. Scheffler, Phys. Rev. Lett. **92**, 046101 (2004).
[26] G. Ketteler, D. F. Ogletree, H. Bluhm, H. Liu, E. L. D. Hebenstreit, and M. Salmeron, J. Am. Chem. Soc. **127**, 18269 (2005).
[27] J. Klikovits, M. Schmid, L. R. Merte, P. Varga, R. Westerström, A. Resta, J. N. Andersen, J. Gustafson, A. Mikkelsen, E. Lundgren, F. Mittendorfer, and G. Kresse, Phys. Rev. Lett. **101**, 266104 (2008).
[28] H. Over, Y. D. Kim, A. P. Seitsonen, S. Wendt, E. Lundgren, M. Schmid, P. Varga, A. Morgante, and G. Ertl, Science **287**, 1474 (2000).
[29] B. L. M. Hendriksen and J. W. M. Frenken, Phys. Rev. Lett. **89**, 046101 (2002).
[30] M. D. Ackermann, T. M. Pedersen, B. L. M. Hendriksen, O. Robach, S. C. Bobaru, I. Popa, C. Quiros, H. Kim, B. Hammer, S. Ferrer, and J. W. M. Frenken, Phys. Rev. Lett. **95**, 255505 (2005).
[31] J. Gustafson, R. Westerström, A. Mikkelsen, X. Torrelles, O. Balmes, N. Bovet, J. N. Andersen, C. J. Baddeley, and E. Lundgren, Phys. Rev. B **78**, 045423 (2008).
[32] J. I. Flege and P. Sutter, Phys. Rev. B **78**, 153402 (2008).
[33] R. Westerström, J. G. Wang, M. Ackermann, J. Gustafson, A. Resta, A. Mikkelsen, J. N. Andersen, E. Lundgren, O. Balmes, X. Torrelles, J. W. M. Frenken, and B. Hammer, J. Phys.: Condens. Matter **20**, 184018 (2008).
[34] Y. B. He, M. Knapp, E. Lundgren, and H. Over, J. Phys. Chem. B **109**, 21825 (2005).
[35] J. Aßmann, D. Crihan, M. Knapp, E. Lundgren, E. Löffler, M. Muhler, V. Narkhede, H. Over, M. Schmid, A. P. Seitsonen, and P. Varga, Angew. Chem., Int. Ed. **44**, 917 (2005).
[36] H. Over, O. Balmes, and E. Lundgren, Surf. Sci. **603**, 298 (2009).
[37] G. Ertl and P. Rau, Surf. Sci. **15**, 443 (1969).
[38] M. Jo, Y. Kuwahara, M. Onchi, and M. Nishijima, Chem. Phys. Lett. **131**, 106 (1986).
[39] J. Goschnik, M. Wolf, M. Grunze, W. N. Unertl, J. H. Block, and J. Loboda-Cackovic, Surf. Sci. **178**, 831 (1986).
[40] J.-W. He and P. R. Norton, Surf. Sci. **230**, 150 (1990).
[41] H. Niehus and C. Achete, Surf. Sci. **369**, 9 (1996).
[42] M. Nishijima, M. Jo, Y. Kuwahara, and M. Onchi, Solid State Commun. **60**, 257 (1986).
[43] B. Brena, G. Comelli, L. Ursella, and G. Paolucci, Surf. Sci. **375**, 150 (1997).
[44] G. Comelli, M. Sastry, G. Paolucci, K. C. Prince, and L. Olivi, Phys. Rev. B **43**, 14385 (1991).
[45] H. Tanaka, J. Yoshinobu, and M. Kawai, Surf. Sci. **327**, L505 (1995).
[46] R. A. Bennett, S. Poulston, I. Z. Jones, and M. Bowker, Surf. Sci. **401**, 72 (1998).
[47] J.-W. He, U. Memmert, K. Griffiths, and P. R. Norton, J. Chem. Phys. **90**, 5082 (1989).
[48] K. Yagi, K. Higashiyama, and H. Fukutani, Surf. Sci. **295**, 230 (1993).
[49] N. Takagi, Y. Yasui, M. Sawada, A. Atli, T. Aruga, and M. Nishijima, Chem. Phys. Lett. **232**, 531 (1995).
[50] K. Yagi and H. Fukutani, Surf. Sci. **412-413**, 489 (1998).
[51] M. Kralj, T. Pertram, N. Seriani, C. Becker, A. Krupski, F. Mittendorfer, and K. Wandelt, Surf. Sci. **602**, 3706 (2008).
[52] R. Westerström, C. J. Weststrate, A. Resta, A. Mikkelsen, J. Schnadt, J. N. Andersen, E. Lundgren, M. Schmid, N. Seriani, J. Harl, F. Mittendorfer, and G. Kresse, Surf. Sci. **602**, 2440 (2008).
[53] V. A. Bondzie, P. H. Kleaban, and D. J. Dwyer, Surf. Sci. **465**, 266 (2000).
[54] J. Han, D. Y. Zemlyanov, and F. H. Ribeiro, Surf. Sci. **600**, 2730 (2006).
[55] A. I. Titkov, A. N. Salanov, S. V. Koscheev, and A. I. Boronin, Surf. Sci. **600**, 4119 (2006).
[56] R. Nyholm, J. N. Andersen, U. Johansson, B. N. Jensen, and I. Lindau, Nucl. Instrum. Methods Phys. Res. A **520**, 467 (2001).
[57] A. Stierle, A. Steinhäuser, A. Rühm, F. U. Renner, R. Weigel, N. Kasper, and H. Dosch, Rev. Sci. Instrum. **75**, 5302 (2004).
[58] S. Ferrer and F. Comin, Rev. Sci. Instrum. **66**, 1674 (1995).
[59] J. P. Perdew, J. A. Chevary, S. H. Vosko, K. A. Jackson, M. R. Pederson, D. J. Singh, and C. Fiolhais, Phys. Rev. B **46**, 6671 (1992).
[60] P. E. Blöchl, Phys. Rev. B **50**, 17953 (1994).
[61] G. Kresse and D. Joubert, Phys. Rev. B **59**, 1758 (1999).
[62] G. Kresse and J. Furthmüller, Comput. Mater. Sci. **6**, 15 (1996).
[63] L. Köhler and G. Kresse, Phys. Rev. B **70**, 165405 (2004).
[64] S. Doniach and M. Šunjić, J. Phys. C **3**, 285 (1970).
[65] G. K. Wertheim and P. H. Citrin, *Photoemission in Solids I*, Topics in Applied Physics Vol. 26, (Springer-Verlag, Berlin, 1978).
[66] J. N. Andersen, D. Hennig, E. Lundgren, M. Methfessel, R. Nyholm, and M. Scheffler, Phys. Rev. B **50**, 17525 (1994).
[67] E. Vlieg, J. Appl. Crystallogr. **30**, 532 (1997).
[68] E. Vlieg, J. Appl. Crystallogr. **33**, 401 (2000).
[69] International Union of Crystallography, *International Tables for X-ray Crystallography* (Kynoch, Birmingham, 1968), Vol. III.
[70] $B=8/3\pi^2u^2$, where u^2 is the mean-square vibrational amplitude of the atoms.
[71] O. L. Warren and P. A. Thiel, Phys. Rev. B **47**, 10848 (1993).
[72] J. E. Houston and R. L. Park, Surf. Sci. **21**, 209 (1970).
[73] M. S. Altman, Surf. Sci. **344**, 65 (1995).
[74] T. Ohtani, K. Tamiya, Y. Takeda, T. Urano, and S. Hongo, Appl. Surf. Sci. **130-132**, 112 (1998).
[75] G. Zheng and E. I. Altman, Surf. Sci. **504**, 253 (2002).
[76] H. H. Rotermund, Surf. Sci. Rep. **29**, 265 (1997).